Molecular Modelling of Carboranes using Distance Restraints: The Molecular Dynamics Simulation of Appended Thioether Macrocycles *

John D. Holbrey,[a] Peter B. Iveson,[a] Joyce C. Lockhart,[a] Nicholas P. Tomkinson,[a] Francesc Teixidor,[b] Antonio Romerosa,[b] Clara Viñas[b] and Jordi Rius[b]

[a] *Department of Chemistry, The University, Newcastle upon Tyne, NE1 7RU, UK*

[b] *Institut de Ciencia de Materials de Barcelona, Consejo Superior de Investigaciones Cientificas, Campus UAB, Bellaterra 08913, Spain*

A molecular mechanics model for *o*-carborane cages has been developed, using distance restraints to hold the polyhedron in position. The combination of *o*-carborane cage interatomic distance restraints (a modified central force field) and CHARMm parameters gives a good representation of the carborane cage geometry. Molecular dynamic simulations of macrocyclic thioethers ligated to the carbons of the carborane have been carried out. The rigid cage section seems to provide an accessible interconversion route between conformers of the macrocycle, effectively an entatic state. The new carborane 1,2-(6'-oxa-3',9'-dithiaundecane-1',11'-diyl)-1,2-dicarba-*closo*-dodecaborane, the four-step synthesis and crystal structure of which are presented, provided a contrasting macrocyclic appendage with thioethers indirectly linked to the *o*-carborane cage through ethane bridges. Molecular dynamics simulation of this molecule was also carried out.

The molecular mechanics (MM) or force field method for simulating chemical structural behaviour was originally developed to deal with organic molecules,[1-3] particularly those for which the notion of a bond between two atoms was a viable concept. It generally uses the conventional representation of the simple single bond as a vector joining two atoms, which is often sufficient for the descriptive needs of most organic chemists. The enormous success of the method in accounting for organic structures and the general acceptance of the predictive value of the method is in part due to the insights gained by the practitioners of the method into the competing demands of various forces used in the force field—bond stretching, angle bending, torsions, van der Waals and coulombic interactions.[4] However, the method is less simple to apply to compounds of elements which have a geometry differing from the usual organic range—for example, metallocenes, soft metal ions or polyhedral molecules. For metal ions in general, where co-ordination numbers are greater than four, and even four-co-ordinate metal ions in square planar environments, it is clumsy to apply the angle and torsion contributions adequately (but see a new force field describing square-planar Pt[5]). For polyhedral cage compounds where the concept of a two-centre two-electron bond described with a simple vector is certainly not viable, a new approach must be found. In our recent work with thioether macrocycles, we have been faced with both of these problems. Work on metal-ion force fields for thioether macrocycles[6,7] will be reported separately. In this paper we describe an approach to simulation of thioxaether macrocycles which have as a ring component a carborane cage, novel molecules with tremendous potential for catalysis, for production of polymers with special characteristics, and in nuclear medicine, some of which have been described elsewhere.[8-11] These molecules combine a soft 7,8-dicarba-*nido*-undecaborate(1−) or 1,2-dicarba-*closo*-dodecaborane unit with 9-, 12- and 15-membered ring macrocycles containing hard and soft donor atoms.

Polyhedral borane cages have been a major focus of inorganic chemistry for several decades.[12-14] Crystallographic (and even neutron diffraction) data on borane and carborane cages are available in great quantity [*e.g.* over 60 icosahedral carborane structures in the latest update of the Cambridge Structural Database (as implemented on CDS at Daresbury)[15]] and sufficient structures of the molecules it was intended to simulate were available to provide the necessary geometric data. Likewise, electrostatic potentials have been calculated with every quantum mechanical method possible, so that there is general understanding of the electron distribution within the cages. To construct a force field to represent carboranes remains, however, a considerable challenge, because of the inapplicability of 'two-centre' bonding concepts.† Since the customary force-field approach would require such a tedious number of parameters, it was decided to use as a preliminary approach, the distance restraint method, which has been used in protein modelling for example, to supply nuclear Overhauser effect (NOE) information on distances between nuclei (obtained from NMR investigations).[17] It should be appreciated that both the force field approach and the distance restraint approach are based on highly artificial models of a molecule. The approximation used here was to set all the force constants for the force field to zero in respect of the heavy cage atoms, controlling these purely through the distance restraints, while using the full force field for the macrocycle portions. The approach for the polyhedral part is similar to the pure central force field employed by Saunders and Jarret[18] in their STRFIT software, which they applied to a polyhedral carbon compound amongst others; this uses a force only along the line joining two atoms. We reasoned that in later consideration of the geometry of the cage-derivatised macrocycles, the cage would have a fairly rigid geometry, and that its effect on the rest of the molecule would most likely be through electrostatic and van der Waals

* *Supplementary data available:* see Instructions for Authors, *J. Chem. Soc., Dalton Trans.*, 1993, Issue 1, pp. xxiii–xxviii.

Non-SI unit employed: cal ≈ 4.184 J.

† For example, in the *closo*-carborane cage shown in Fig. 1, all B and C atoms are six-connected, to five other cage atoms, and one *exo* atom. This creates problems with angle and torsion terms, requiring many additional parameters for a standard CHARMm force field representation.

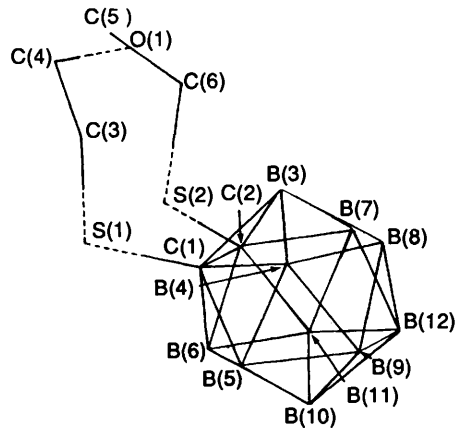

1

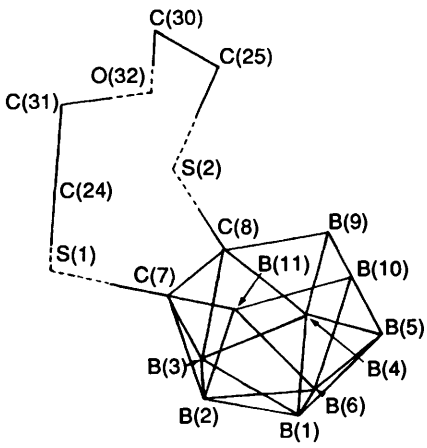

2

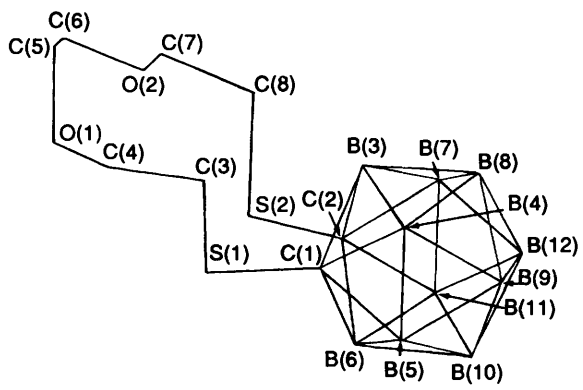

3

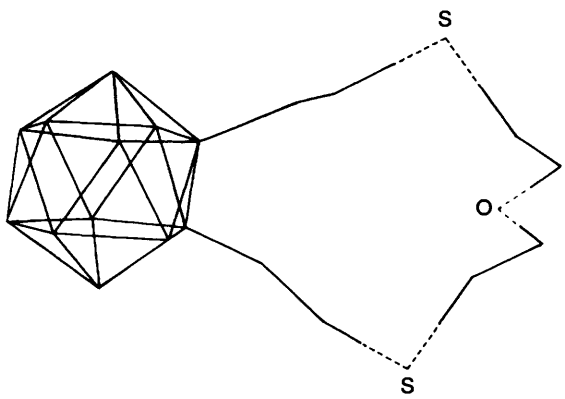

4

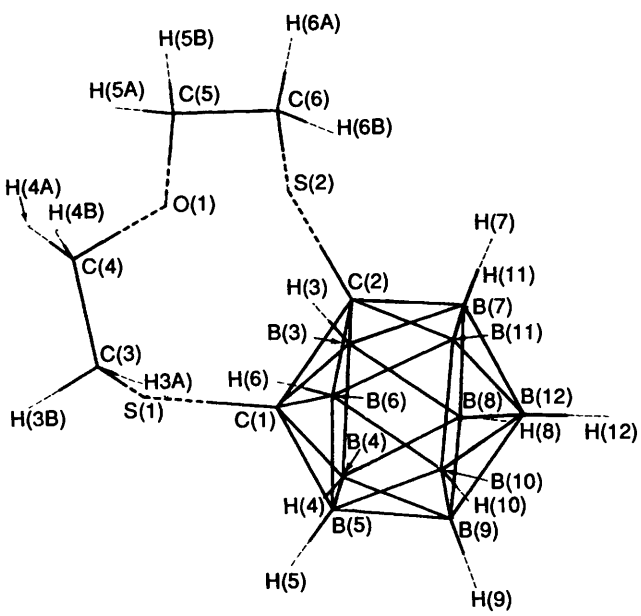

Fig. 1 Numbering of the atoms in the carborane cage of **1**, including hydrogens

interactions, which would be adequately represented by our approach. The results reported here indicate that the effect of the cage on the rest of the molecule can in principle be described by the relatively crude restraint approximation. Kepert and co-workers[19,20] approached the problem of simulating borane cages differently; at present we do not envisage incorporation of this approach within the model we have adopted.

Table 1 Assignment of atom types for CHARMm for the *o*-carborane cage

Atom type	Atoms*	Description
BT(1)	B(6), B(3)	Attached to C(1) and C(2)
BT(2)	B(5), B(4), B(11), B(7)	Attached to either C(1) or C(2)
BT(3)	B(9), B(12)	In same mirror plane as C(1) and C(2)
BT(4)	B(8), B(10)	Attached to types BT(2) and BT(3)

* Labelled as in Fig. 1.

Method

The software available was the CHARMm force field[16] (version 21.3) supplied by Polygen, and running on SG IRIS 4D20G machines. Since this force field contained only van der Waals parameters for boron, a provisional set of distance restraints and force field parameters, designed to reproduce the cage geometry as determined in the crystal, was added as follows: consensus geometries required were taken from literature compilations and the SERC CDS implementation (Daresbury) of the Cambridge Crystal Structure Database.[15] Distance restraints were used to replicate the carborane cage geometry while the associated B–H bonds and angles were described using force field parameters.

Atom Types for the Boron Cages.—The neutral thioxaether cage compounds examined were 1,2-(3′-oxapentanediyldithio)-1,2-dicarba-*closo*-dodecaborane[8] **1**, 1,2-(3′,6′-dioxaoctanediyldithio)-1,2-dicarba-*closo*-dodecaborane[9] **3**, and the new compound, described in the Experimental section, 1,2-(6′-

Table 2 Assignment for atom types for CHARMm for the 7,8-dicarba-*nido*-undecaborate(1 −) cage

Atom type	Atoms*	Description
BT(1)	B(3)	Attached to C(7) and C(8)
BT(2)	B(4), B(2)	Non-facial B bonded to either C(7) or C(8)
BT(3)	B(5), B(6)	Attached to BT(4), BT(5) and BT(2)
BT(4)	B(1)	Attached to types BT(2), BT(3) and BT(1)
BT(5)	B(9), B(11)	Facial B bonded to either C(7) or C(8)
BT(6)	B(10)	Facial B bonded to type BT(5)

* Labelled as in Fig. 2.

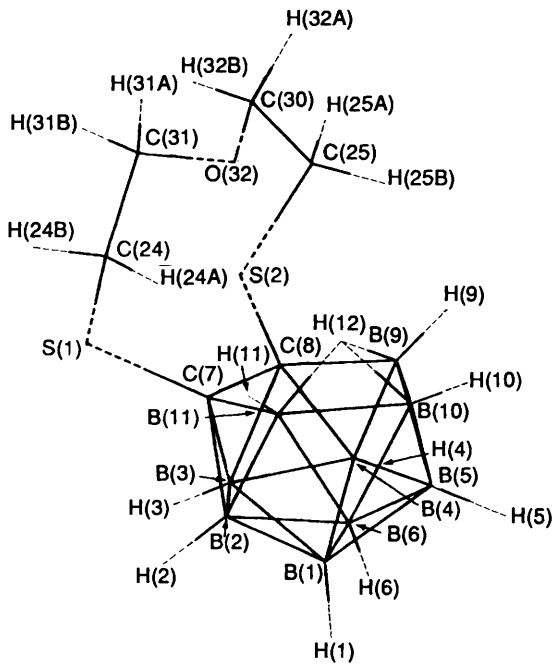

Fig. 2 Numbering of the atoms in the carborane cage of **2**, including hydrogens

oxa-3′,9′-dithiaundecane-1′,11′-diyl)-1,2-dicarba-*closo*-dodecaborane **4**. For these carboranes there are four different boron environments, as shown from ^{11}B NMR spectroscopy; for our purposes, these were labelled types BT(1)–BT(4) and can be identified through symmetry as shown in Table 1. The numbering system for this cage is shown in Fig. 1.

The anionic compounds examined were the anions of the degradation products of the carborane cages in the preceding section, namely sodium 7,8-(3′-oxapentanediyldithio)-7,8-dicarba-*nido*-undecaborate(1 −) **2**, and the trimethylammonium salt of the 7,8-(3′,6′-dioxaoctanediyldithio)-7,8-dicarba-*nido*-undecaborate(1 −)[9] anion **5**. For these anionic dicarba-*nido*-undecaborates, the symmetry is lowered and six different boron environments are identified, BT(1)–BT(6), which correspond to the boron types for the $B_{10}C_2$ *o*-carboranes and two types describing the open face of the B_9C_2 *nido* compounds, outlined in Table 2. The atom numbering for this cage is shown in Fig. 2.

Up to seven different B–B bond types can be identified for each of the two types of carborane cage and 'consensus' bond lengths defined for these based on average bond lengths from crystallographic sources (see Tables 3 and 4). Two B–C and one C–C bond length(s) for the *o*-carborane cage ($B_{10}C_2$) were also identified.

In general, the B–B and B–C separations for the carborane are reproducible from one crystal structure to another (see below). Problems were posed by the C–C distance for the *closo*-carborane cage: a range of values ranging from 1.49 to 1.86 Å

Table 3 Bond lengths used in CHARMm for *o*-carboranes

Bond type*	Bond length Set 1	Bond length Set 2
BT(1)–BT(2)	1.80	1.77
BT(1)–BT(4)	1.77	1.77
BT(2)–BT(2)	1.78	1.78
BT(2)–BT(3)	1.77	1.78
BT(2)–BT(4)	1.77	1.77
BT(3)–BT(3)	1.77	1.77
BT(3)–BT(4)	1.79	1.79
BT(1)–C	1.73	1.72
BT(2)–C	1.70	1.70
C–C	1.82	1.67

* Based on atom types defined in Table 1.

Table 4 Bond lengths used in CHARMm for 7,8-dicarba-*nido*-undecaborate(1 −)

Bond type*	Bond length/Å	Bond type*	Bond length/Å
C–C	1.58	BT(2)–BT(4)	1.79
C–S	1.78	BT(2)–BT(5)	1.79
C–BT(2)	1.67	BT(3)–BT(3)	1.81
C–BT(5)	1.65	BT(3)–BT(4)	1.76
C–BT(1)	1.72	BT(3)–BT(5)	1.76
BT(1)–BT(2)	1.74	BT(3)–BT(6)	1.80
BT(1)–BT(4)	1.76	BT(5)–BT(6)	1.80
BT(2)–BT(3)	1.75		

* Atom types defined in Table 2.

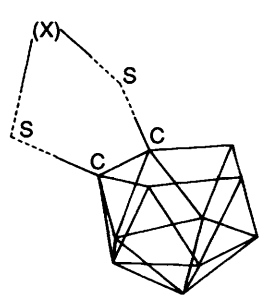

X
5 $(CH_2CH_2O)_2CH_2CH_2$
6 $(CH_2CH_2O)_3CH_2CH_2$

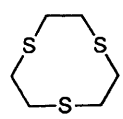

7

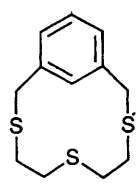

8

has been reported for this distance. A value calculated by Ott and Gimarc[21] using *ab initio* methods [Slater type orbital STO-3G set] is 1.634 Å. The origin of the values determined crystallographically was examined. Where the C–C formed one edge of a triangle completed by a metal ion, the distance was short, with a mean of 1.61 Å, standard deviation (s.d.) 0.04, n = 32. The other structures examined gave a mean value of 1.70 Å, s.d. 0.06, n = 27. Longer average lengths were quoted in work at −120 °C (C–C 1.685 Å, s.d. = 0.03, n = 8). Unfortunately the thioether macrocyclic derivatives we wanted to investigate all had crystallographically determined C–C lengths at the longer extreme even of this range. The distances to which these structures were restrained are quoted in Table 3 (as set 1). A second set of distance restraints (set 2) is also given in this Table, containing the more general average of the *closo* cage structures found in the database; the value for the C–C bond length in this set was determined for all non-metal cages, but excluding the values over 1.8 Å, used for set 1. Another relevant feature is the number of distance restraints required. For a perfect icosahedral structure with all heavy atoms equivalent, the central forces acting along

Table 5 Charges used for carborane simulations

o-Carborane **1** overall charge 0.000		Undecaborate **2** overall charge −1.000	
Atom[a]	Charge	Atom[b]	Charge
S(1)	−0.049	S(2)	−0.135
S(2)	−0.053	S(1)	−0.150
C(1)	0.178	C(7)	0.037
C(2)	0.174	C(8)	0.036
B(3)	0.062	B(1)	−0.023
B(4)	0.030	B(2)	0.022
B(5)	0.039	B(3)	0.101
B(6)	0.068	B(4)	0.018
B(7)	0.034	B(5)	0.004
B(8)	−0.001	B(6)	0.002
B(9)	0.006	B(9)	0.007
B(10)	0.002	B(10)	−0.111
B(11)	0.040	B(11)	0.003
B(12)	0.016	H(1)	−0.109
O(1)	−0.239	H(2)	−0.108
H(3)	−0.067	H(3)	−0.113
H(4)	−0.068	H(4)	−0.109
H(5)	−0.069	H(5)	−0.111
H(6)	−0.067	H(6)	−0.112
H(7)	−0.070	H(9)	−0.117
H(8)	−0.080	H(10)	−0.085
H(9)	−0.074	H(11)	−0.116
H(10)	−0.083	H(12)	0.218
H(11)	−0.068	C(24)	−0.055
H(12)	−0.090	H(24A)	0.035
C(3)	−0.049	H(24B)	0.005
H(3A)	0.075	C(25)	−0.054
H(3B)	0.045	H(25A)	0.035
C(4)	0.139	H(25B)	0.008
H(4A)	0.021	C(30)	0.184
H(4B)	−0.013	H(30A)	−0.033
C(5)	0.172	H(30B)	−0.046
H(5A)	−0.018	C(31)	0.184
H(5B)	−0.010	H(31A)	−0.044
C(6)	−0.041	H(31B)	−0.031
H(6A)	0.047	O(32)	−0.238
H(6B)	0.058		

[a] Labelled as in Fig. 1. [b] Labelled as in Fig. 2.

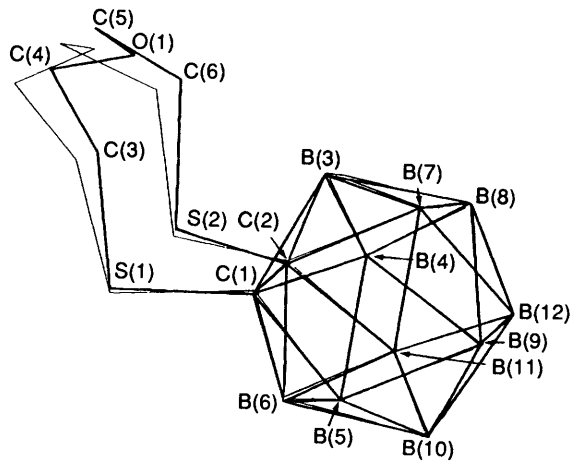

Fig. 3 Superposition and fit of the minimised carborane geometry of **1** obtained using the force field, with that of the unminimised crystal structure[8]

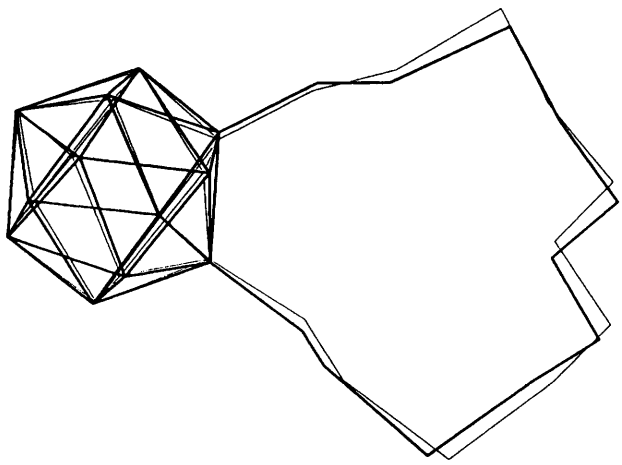

Fig. 5 Superposition and fit of minimised geometry of **4** with that of unminimised crystal structure

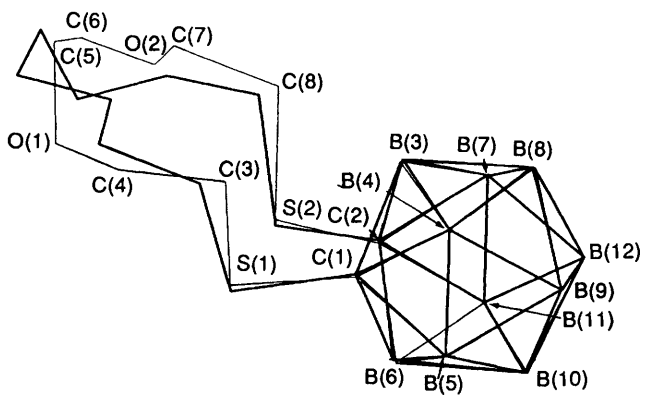

Fig. 4 Superposition and fit of the minimised geometry of **3** with that of the unminimised crystal structure[10]

each side of the triangular faces of the polyhedron will produce a perfect icosahedron. However, even in the 1960s, it was evident from crystal data[22-24] that the distance between apical atoms of the *o*-carborane cage was different when apical C,B pairs were chosen (ideal 3.23 Å is given by Potenza and Lipscomb[22,23]) than when apical B,B pairs were chosen (ideal 3.34 Å). This is a general feature of all the structures in the database which we examined, and reflects the shorter C–C bond, and the shorter C–B bonds, relative to the B–B bond distances. Thus any mild discrepancy in *e.g.* the C–C or C–B distances could be corrected by addition of an appropriate distance restraint between C,B apical atoms of the icosahedron, or changing the restraint constants for specific distances. This approach will be the subject of future work. Corresponding distance restraints for the 7,8-dicarba-*nido*-undecaborate(1−) unit are given in Table 4.

Complete neglect of differential overlap (CNDO) charges were calculated for each structure after initial ABNR (adopted basis Newton Raphson) minimisation, examples being shown in Table 5; these were used for subsequent minimisations.

CHARMm Force Field.—Certain other parameters required in CHARMm (force constants for bonds, angles and torsions for the cage) were left at zero so that the geometry of the cage was controlled entirely by the restraint forces, van der Waals and coulombic interactions. This produces a similar result to that from the more usual force field approach, but neglecting all the angle and torsion terms. It has been developed to apply distance information obtained from various NMR techniques such as NOE and paramagnetic relaxation in the molecular modelling

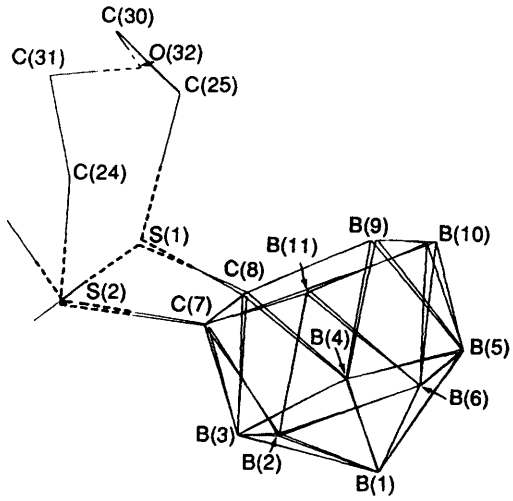

Fig. 6 Superposition and fit for *nido*-carbaborate **2** *versus* cage of **6** (ref. 8)

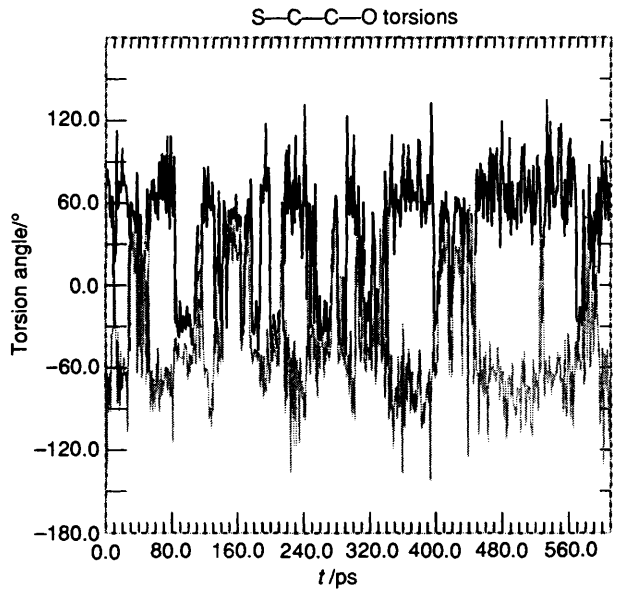

Fig. 7 Time evolution during MD simulation of the S–C–C–O torsions of compound **1**

of proteins and is available within the commercial software used; use of the software is easily adapted to apply a central force field. Both this and the more usual valence force field approach are completely artificial ways of describing the forces on a molecule, and are justified only if they reproduce reasonably various properties of the molecule. The restraint forces for the neutral and the anionic cages described in this work were applied according to equations (1)–(3) (below). The energy term within CHARMm for a restraint to keep two atoms A and B within a certain distance of each other takes the form of equation (1) where r is the distance between atoms A

$$E = k(r - r_0)^2 \quad (1)$$

and B, and r_0 is the restraint distance. The force constant (k) is defined as in equations (2) and (3) for $r > r_0$ and $r < r_0$

$$k = 0.5Sk_bT/(r - r_0)^2 \quad (2)$$

$$k = 0.5Sk_bT/(r_0 - r)^2 \quad (3)$$

respectively, where k_b is the Boltzmann constant, T the temperature (Kelvin), S is a scaling factor, usually unity. At distance r_0 the value of the restraint energy is $0.5Sk_bT$. The restraint distances were those given in Tables 3 or 4, as appropriate. Initial values of $|r_0 - r|$ tried were ±0.01, 0.015, 0.02, 0.025 and 0.03 Å; T was kept at 300, and S at 1, while the value used for $|r_0 - r|$ for the simulations reported was 0.02 Å. These simulations were of molecules *in vacuo*; although crown thioethers are believed to be much less susceptible to solvent effects than oxygen crown ethers, future work should tackle the computationally more intensive situation in which solvent effects are modelled.

Calibration.—The crystal data for thiomacrocycle molecules **1**, **3** (representing the *closo* cage) and **6** (representing the undecaborate cage) were available for calibration, while compound **4** was synthesised by the route shown in Scheme 1 (see later), and its crystal structure obtained in order to provide a comparison with a different mode of attachment of the macrocycle thioether ring to the carborane cage. The restraints (Tables 3, set 1, and Table 4) for appropriate models were tested against the known geometries of **1**, **3**, **4** and **6**. Molecular mechanics minimisations with any of these gave structures in agreement with the crystal data. The *closo*-C_2B_{10} cages (compounds **1**, **3**, **4**) gave structures which fitted the crystal data (cage part only) as shown in Figs. 3, 4 and 5 respectively, with total root mean square (r.m.s.) deviations of 0.0440, 0.0455 and 0.1285 Å respectively, over the heavy atoms of the cage, plus the two attached sulfurs (14 atoms for **1** or **3**, or cage only for **4**); the model of the open-face anionic undecaborate cage fitted the crystal structure of analogous compound[9] **6** (cage portion only) with r.m.s. deviation of 0.07 Å, and the superposition of the cages is shown in Fig. 6. In each case a rigid body fit as described in the QUANTA manual was used for the comparison. The more general class of distance restraints shown in Table 3 as set 2 for the generalised geometry of the *closo* cages was used to minimise the structure of **1**; the resultant minimised structure was fitted to the unminimised crystal structure of **1**, and the fit was 0.0397 Å.

Molecular Dynamics.—The molecular dynamics (MD) protocol developed for simulation of thioether macrocycles[25] was used for MD simulations. In the earlier work, it was convenient to represent the voluminous output from the computations in terms of the time-evolution of certain geometrical features, such as distances between non-bonded atoms,[26] or torsion angles of thioether segments.[25] Torsion angles have generally been chosen to describe the geometry variations found in this work. Simulations were usually run for 600–1000 ps. Comparison of the results for **1** and **2**, was made, so that the effect of the open-face *versus* the *closo* carborane cage on the movement of the crown ether moiety could be examined. The effect of changing the distance tolerance $r - r_0$ (or $r_0 - r$) of the restraint [see equations (1)–(3)] to the values 0.01, 0.02 and 0.03 Å was investigated. Compound **4** provided another extension of the molecular types examined, with a link of two carbon atoms separating the sulfurs from the cage carbons. This is expected to be a much less restricted molecule than **1**, so that the comparison of the results for **1** and **4** was of some interest.

Results

For the neutral carborane **1**, MM minimisation incorporating the restraint parameters gave a cage structure very close to the actual crystal structure (unminimised).[8] The two are shown superposed and fitted in Fig. 3. For molecules **3** and **4**, MM minimisations also compared satisfactorily with the crystal structures, as shown in Figs. 4 and 5. The 7,8-dicarba-*nido*-undecaborate(1−) cage (modelled as **2**) also gave a good fit with the cage structure found in the crystal data[9] of **6**; the superposition of the modelled cage and the crystal structure of the cage of **6** is shown in Fig. 6. The general representation of the cage was thus considered satisfactory for further work with

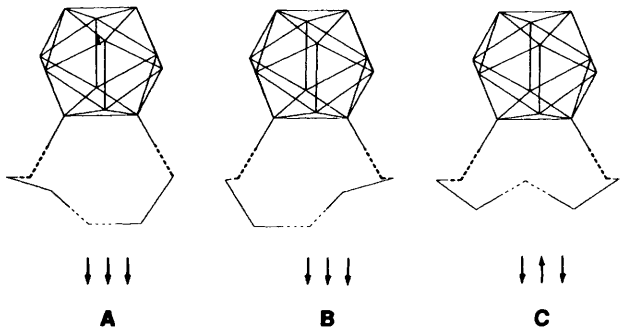

Fig. 8 Sections A, B and C, from the simulation from Fig. 7, after being averaged and subsequently minimised. The calculated MM energy (kcal mol^{-1}) and S–C–C–O torsions (°) of **A**, **B** and **C** were 11.10, −53.31, −29.48; 11.06, 53.41, 2.952; 11.31, 66.08, −66.61 respectively

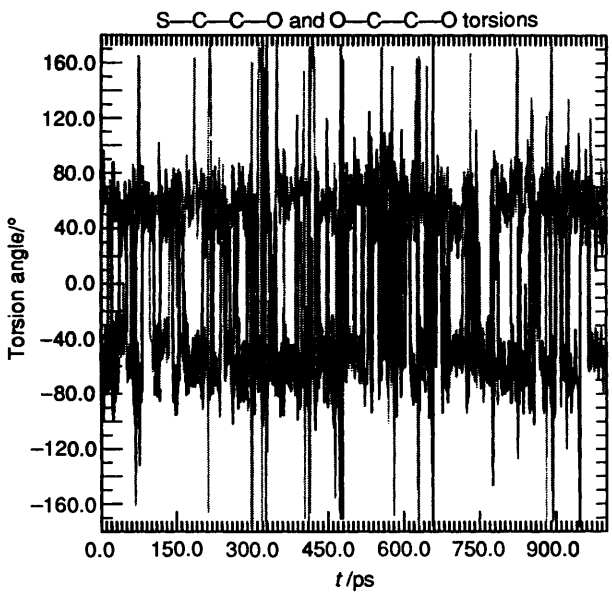

Fig. 9 Time evolution during MD simulation of the S–C–C–O and O–C–C–O torsions of the *closo*-carborane **3**

dynamics on the more mobile macrocycle sections of the compounds **1**–**6**.

MD simulation of carborane **1**. Time evolution of the S–C–C–S torsion angle, at the junction of the carborane and the macrocycle portions of **1**, indicated that on the time-scale of the simulations (ps to ns) this scarcely moved. Such a feature is likely to be dominant in the movement of an otherwise fluxional macrocyclic ring. The two distinct torsion angles for the S–C–C–O atoms varied with simulation time as shown in Fig. 7. Scatter plots of these torsions showed three distinct clusters of structures, with dihedral angles in the range 60/−60, 50/25, −25/ −50°. The average structure of each cluster was minimised to provide three structures shown in Fig. 8, along with the calculated MM energies. The structure **A** of lowest energy is essentially that found in the crystal structure, with both sulfurs pointing down, and the O pointing up (relative to the carborane C–C bond axis, and viewing the B(3) atom as the upper apex of the *closo* cage). The latter two conformers (**B** and **C**), with all three donor atoms pointing down, are essentially enantiomeric, and are likely to be suitable for complexation. The traces in Fig. 7 are of interest, in relation to those found[25] for the prototype trithiacyclononane thioether, 1,4,7-trithiacyclononane **7**, which underwent torsional change somewhat slowly by comparison. In Fig. 7 there are no long-lived transients, with the molecule in continuous rapid movement on this timespan. The simulated nonane **7** apparently passed through conformations with one torsion close to zero but these were extremely short-lived transients and potentially intermediates on the reaction coordinate for fluxional change: the common conformers of **7**, which had all-*gauche* S–C–C–S torsions, existed for timespans of 100 ps or more. Since the carborane cage essentially fixes the single S–C–C–S torsion of **1** close to zero (*cf.* S–C–C–S where C–C is part of a benzene ring), equating to the unstable transients of **7**, the whole molecule **1** is likely to be in a permanent entatic state, and thus mobile, compared to the simple cyclononane, **7**, as is observed in the simulation. This result at first seemed anomalous, since the rigid cage might be expected to hold the structure static and damp any movement. However, from the viewpoint of MD simulation, the unfavourable S–C–C–S torsion associated with the cage promotes compensatory movement elsewhere in the molecule. This interesting result may be of general relevance in consideration of the entatic state in biological molecules.

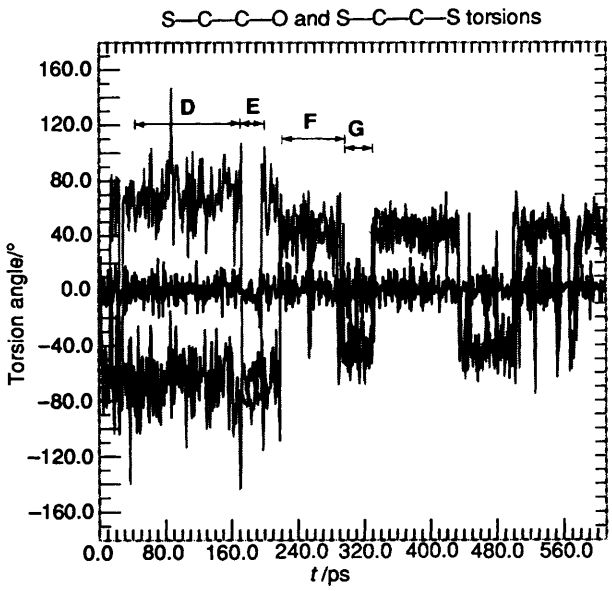

Fig. 10 Time evolution during MD simulation of the S–C–C–O and S–C–C–S torsions for the *nido*-carbaborate(1 −) structure **2**, starting from the structure built from **6**, giving sections **D**, **E**, **F** and **G**

Results for carborane **3**. Three torsions (two S–C–C–O and O–C–C–O) were considered (in the modelling output shown in Fig. 9). For all three, regardless of whether donor atoms were O or S, the torsional transitions observed were from *gauche* to *gauche*, with remarkably few *anti* conformations. The crystal structure conformation[8] is seen in around 20% of the simulated conformations. In accord with the findings for **1**, the macrocycle section of **3** is found to be very mobile, as expected with one torsion maintained close to the eclipsed angle zero.

Results for the nido-*undecaborate cage* **2**. The modelled structure was built using coordinates[8] for the cage atoms of **6**. The built structure, which had one sulfur atom pointing down, away from the carborane open face, and the other up, was only transiently seen in the resultant MD simulation (restraint deviations of ± 0.02). The results were analysed as for **1**, through analysis of clusters of conformers with similar torsion angles. There were four distinct sets of structures. The geometries of the resultant 'averaged' minimised structures (see **D**–**G** on the time-evolution plot of Fig. 10, geometries shown in Fig. 11) should be compared with those of Figs. 7 and 8, to gauge the effect of the open face; the structures of the macrocyclic sections were different to those of Fig. 8, with **E** being unique to this system. Other simulations were started from different conformers (**G**, **D**) obtained from the first simulation. One such simulation started from the conformer labelled **G** in Fig. 11, with both sulfurs and the oxygen pointing down, which was the lowest energy conformer obtained from the starting simulation; the two enantiomers (**F**, **G**) of this structure were the only conformations traversed in this simulation (see results in Fig.

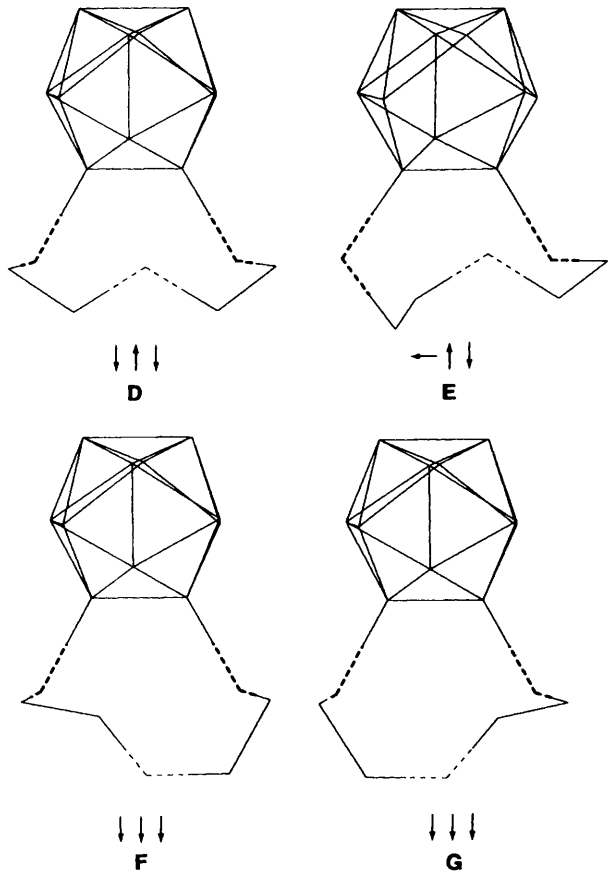

Fig. 11 Structures **D**, **E**, **F** and **G** found from cluster plots of simulation in Fig. 10. The calculated MM energies (kcal mol^{-1}) and S–C–C–O torsions were **D** (43.46, 64.19, −63.73), **E** (46.52, −83.98, −60.82, **F** (42.45, 46.95, 44.88) and **G** (42.44, −45.19, −46.68)

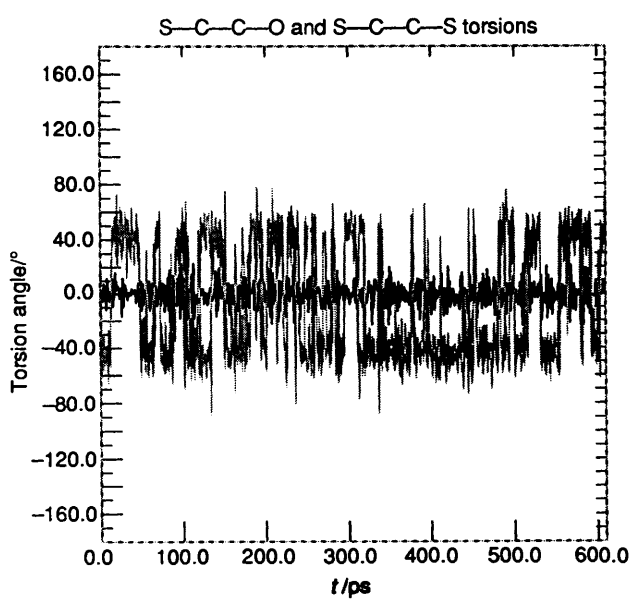

Fig. 12 Time evolution of three torsions (S–C–C–S and S–C–C–O) plotted for the MD simulation of **2**, starting from structure **G**

12). The last simulation was started from the remaining conformer **D**, having the sulfur atoms pointing down, and the oxygen up, towards the open face, analogous to the crystal structure of the related carborane **1**. The results of this are shown in Fig. 13. These three simulations, starting from different points, have shown the likelihood of the resulting

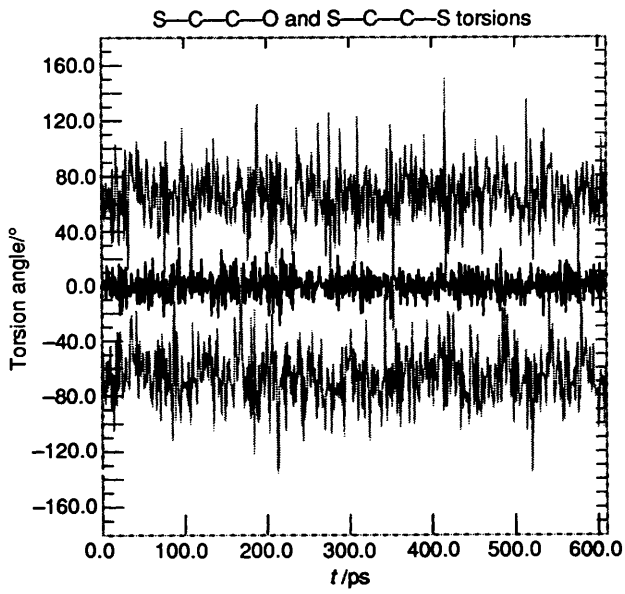

Fig. 13 Time evolution of three torsions (S–C–C–S and S–C–C–O) plotted for MD simulation of **2**, starting from structure **D**

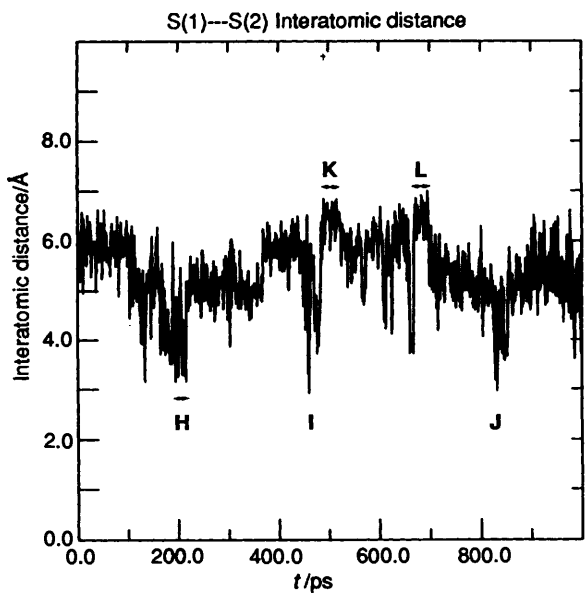

Fig. 14 Time evolution of the S • • • S distance during MD simulation of *closo* cage **4**, starting from the crystal structure coordinates

structures to have the sulfur co-ordination vectors pointing away from the open face (described as *anti* in earlier work [11]). The macrocycles attached to the undecaborate cage (as was the case for **1**) appeared more mobile than those of the simple trithiacyclononane **7**. In relation to the results for **1**, the S–C–C–S torsion in **2** has a slightly less stringent set of forces acting on it, permitting the structure to relax more readily than with compound **1**; the angles of the structures extracted (**D**–**G**) are also more realistically *gauche*.

The structure of **4** was examined by MD starting from the crystal structure coordinates (one component of the disorder only, see the Experimental section). The initial structure was reminiscent of that of the trithia-*m*-benzenophane **8** studied previously;[26] the sulfur atoms were also initially over 6.0 Å apart. Thus, following the presentation of ref. 26, the data are presented as a trace of the distance S • • • S as the simulation proceeds (see Fig. 14). The distance gradually decreases to

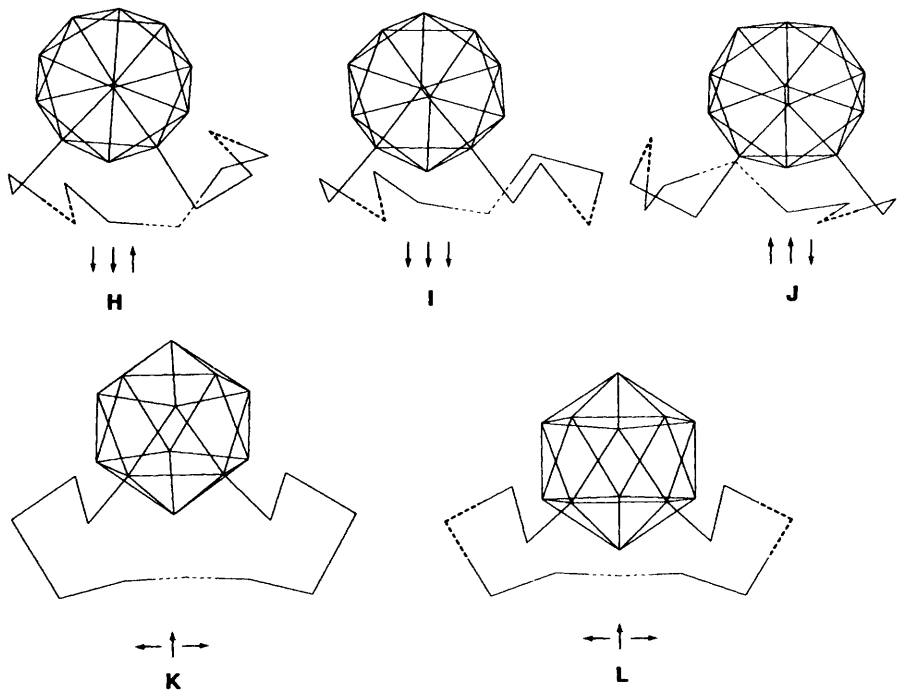

Fig. 15 Structures **H**, **I**, **J**, **K**, **L** obtained from averaging of transients shown in Fig. 14, and subsequent minimisation

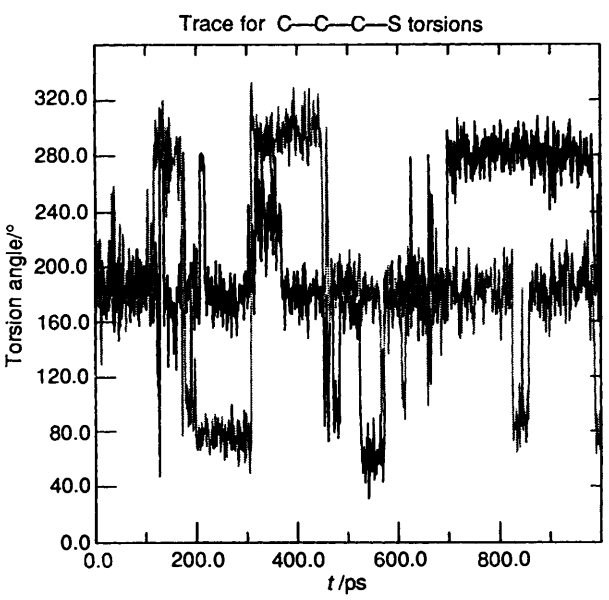

Fig. 16 Trace of the C–C–C–S torsion angles during the MD simulation of the *closo* cage **4**, starting from the crystal structure co-ordinates

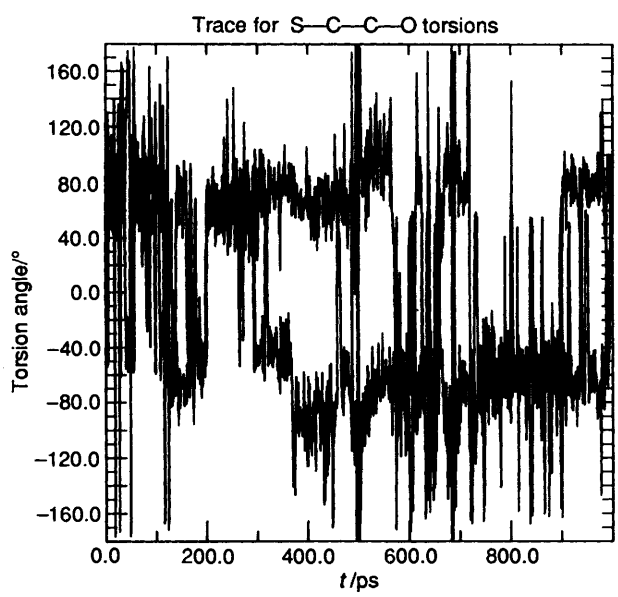

Fig. 17 Trace of the S–C–C–O torsion angles during the MD simulation of compound **4** starting from the crystal structure co-ordinates

around 4.4 Å, and is then in continuous fluctuation between 3.2 and 7.0 Å. The S • • • S distances observed by Teixidor *et al.*[10] in metal chelates of several related species range from 2.78 to 3.23 Å. We thus looked in more detail at the transients with very short (*ca.* 3 Å) and long (7.0 Å) S • • • S distances. Structures with short S • • • S distances (marked as points **H**, **I**, **J** on Fig. 14) and long S • • • S distances (**K**, **L**) were extracted from the dynamics data, minimised, and the resultant structures are shown in Fig. 15. The most stable structure (MM energy 6.4843 kcal mol^{-1}, **I**) has a S • • • S distance of 3.85 Å, and has all three donor atoms (SSO) pointing downwards. Although **H** and **J** have shorter S • • • S distances, the two sulfurs in each case point in opposite directions, and could not co-ordinate intramolecularly to a metal ion. The structures **K** and **L** have *exo* sulfurs, which would not be capable of co-ordinating simultaneously to the same metal ion. The direction of the co-ordination vector of each donor atom (SOS) is indicated beside each structure by means of arrows. It is clear that the structure is more mobile than **1**, probably as a result of the incorporation of the ethano bridges. This is also seen in Figs. 16 and 17, representing the time traces for the torsion angles C–C–C–S, and S–C–C–O respectively, over a 600 ps timescale. The results thus do not define any structure of special stability which might co-ordinate metal ions directly. However, with the greater mobility of the structures, forced by the rigidity of the carborane cage (and relative to those of less rigid macrocycles[25]), rapid rearrangement of the macrocycle portion to co-ordinate a metal ion is likely. At present force fields representing the metal ion co-ordination of such complexes are unavailable. Investigation of the co-ordination will be pursued in more detail when appropriate metal-ion force fields have been established for future work.

Table 6 Refined atomic coordinates ($\times 10^4$) for complex **4** with estimated standard deviations (e.s.d.s) in parentheses

Atom	*X/a*	*Y/b*	*Z/c*	Atom	*X/a*	*Y/b*	*Z/c*
S(1)	7 329(2)	4 231(1)	9 494(1)	C(4A)	9 843(7)	3 665(5)	12 483(5)
S(2)	12 670(2)	2 775(1)	12 171(1)	C(4B)	11 094(14)	4 155(6)	12 592(7)
C(1)	7 492(7)	4 905(3)	12 164(3)	C(5A)	11 649(8)	3 825(6)	12 517(9)
C(2)	9 014(7)	4 540(3)	12 850(3)	C(5B)	10 634(8)	3 146(5)	12 443(6)
B(3)	9 027(8)	5 611(5)	12 435(4)	C(6)	12 988(5)	3 106(3)	11 048(3)
B(4)	7 062(7)	6 012(3)	12 364(3)	C(7)	11 928(6)	2 671(3)	10 340(3)
B(5)	5 852(8)	5 107(4)	12 707(4)	C(8)	9 393(6)	2 706(3)	9 596(3)
B(6)	7 069(9)	4 167(4)	12 980(5)	C(9)	7 705(6)	3 022(3)	9 653(3)
B(7)	9 591(7)	5 373(4)	13 556(4)	C(10A)	8 021(8)	4 735(4)	10 552(3)
B(8)	8 311(7)	6 313(3)	13 279(4)	C(10B)	6 856(12)	4 502(11)	10 614(5)
B(9)	6 355(7)	5 993(4)	13 431(3)	C(11A)	6 928(7)	4 414(4)	11 256(4)
B(10)	6 364(7)	4 838(4)	13 789(4)	C(11B)	8 392(11)	4 798(7)	11 117(8)
B(11)	8 381(7)	4 468(3)	13 875(3)	O	10 374(3)	3 058(2)	10 313(2)
B(12)	7 884(7)	5 596(4)	14 164(3)				

Table 7 Bond lengths (Å) for complex **4** with e.s.d.s in parentheses

S(1)–C(9)	1.808(4)	B(6)–B(10)	1.703(9)
S(1)–C(10A)	1.835(6)	B(6)–B(11)	1.755(7)
S(1)–C(10B)	1.814(7)	B(7)–B(8)	1.775(8)
S(2)–C(5A)	1.844(6)	B(7)–B(11)	1.747(7)
S(2)–C(5B)	1.847(6)	B(7)–B(12)	1.767(7)
S(2)–C(6)	1.810(4)	B(8)–B(9)	1.721(8)
C(1)–C(2)	1.684(6)	B(8)–B(12)	1.758(7)
C(1)–B(3)	1.676(10)	B(9)–B(10)	1.773(7)
C(1)–B(4)	1.688(6)	B(9)–B(12)	1.745(8)
C(1)–B(5)	1.660(9)	B(10)–B(11)	1.762(8)
C(1)–B(6)	1.696(8)	B(10)–B(12)	1.753(8)
C(1)–C(11A)	1.605(7)	B(11)–B(12)	1.761(7)
C(1)–C(11B)	1.804(12)	C(2)–B(3)	1.688(7)
C(4A)–C(5A)	1.519(4)	C(2)–B(6)	1.729(9)
C(2)–B(7)	1.677(7)	C(2)–B(11)	1.677(6)
C(4B)–C(5B)	1.537(5)	C(2)–C(4A)	1.570(8)
C(2)–C(4B)	1.882(12)	C(6)–C(7)	1.497(7)
B(3)–B(4)	1.735(8)	C(7)–O	1.410(5)
B(3)–B(7)	1.780(8)	C(8)–C(9)	1.486(6)
B(3)–B(8)	1.772(8)	C(8)–O	1.423(5)
B(4)–B(5)	1.758(8)	B(4)–B(8)	1.748(7)
C(10A)–C(11A)	1.517(4)	B(4)–B(9)	1.758(7)
B(5)–B(6)	1.743(8)	B(5)–B(9)	1.736(8)
C(10B)–C(11B)	1.517(5)	B(5)–B(10)	1.724(8)

Conclusion

This first attempt to model with a carborane cage has given realistic geometries (*i*) for the cage sections and (*ii*) for the rest of the molecule, and could be used for modelling of cage-containing molecules, *e.g.* carborane polymers and other derivatives similar to those described in this paper. The related *m*-carborane is more thermally stable and is under active investigation as a polymer precursor; the obvious extension of our model to this and other cage and cluster compounds is planned. In particular, our model has allowed assessment of how the open-face *nido* structures permit more rapid movement of the attached macrocycle than do the corresponding *closo* structures, and how both are much more mobile than the corresponding trithiacyclononane. It has also demonstrated transient structures for cage molecules, with sulfur co-ordination vectors *anti* to the open face, as has been found experimentally, and hypothesised by Teixidor *et al.*[9,11] These may be important conformations on the reaction coordinate for interaction with metal ions. It is unrealistic to suppose that any current force field method can simulate reaction, so that other features of boron cages, such as isomerisation, slipping of hydrogen round the open face for example, could not be tackled with this method. The model ignores isomerisation (slow on the NMR time-scale) and H-slipping (fast on the NMR time-scale) since the model uses averaged hydrogen atom positions, corresponding to the observations of the NMR time-scale. This was merely an attempt to permit modelling of the salient features of the molecules. Future work will develop other aspects of modelling with carborane cages. The refining stage[4] for the borane cage is just beginning. Future work will incorporate a metal–sulfur force field to enable study of co-ordination complexes with metals.

Experimental

Before use, 1,2-dicarba-*closo*-dodecaborane (Dexsil Chemical Corporation) was sublimed. All other reagents were from Fluka or Aldrich and were used as supplied. Elemental analyses were performed with a Perkin Elmer 240-B microanalyser. NMR spectra were obtained on a Bruker AM 400WB, and the IR spectra of KBr pellets using a Perkin Elmer 240FT spectrophotometer.

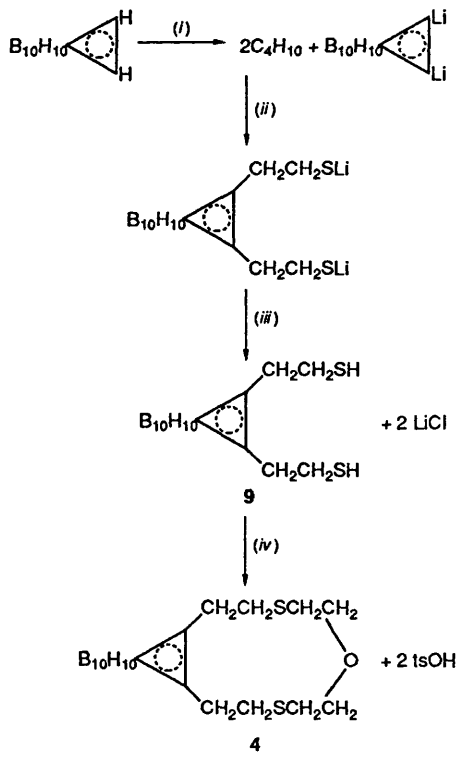

Scheme 1 (*i*) 2LiBu, diglyme, 0 °C, N_2; (*ii*) $\overline{SCH_2CH_2}$, 0 °C, N_2; (*iii*) 2HCl, 0 °C; (*iv*) $tsOCH_2CH_2OCH_2CH_2Ots$, high dilution, ts = *p*-$MeC_6H_4SO_2$

Preparation of 1,2-*Bis*(2-*mercaptoethyl*)-1,2-*dicarba*-*closo*-*dodecaborane* (*Scheme* 1).—To a three-necked round bottom

Table 8 Bond angles (°) for complex **4** with e.s.d.s in parentheses

C(9)–S(1)–C(10A)	103.3(2)	B(3)–B(8)–B(9)	107.3(4)	B(8)–B(12)–B(10)	107.4(3)	C(1)–C(2)–C(4B)	129.4(4)
C(9)–S(1)–C(10B)	97.6(5)	B(4)–B(8)–B(9)	60.9(5)	B(9)–B(12)–B(10)	60.9(4)	B(3)–C(2)–C(4B)	100.0(5)
B(7)–B(8)–B(9)	108.5(4)	B(3)–B(8)–B(12)	107.5(3)	B(7)–B(12)–B(11)	59.4(5)	B(6)–C(2)–C(4B)	143.8(4)
C(5A)–S(2)–C(6)	98.1(5)	B(4)–B(8)–B(12)	108.9(3)	B(8)–B(12)–B(11)	107.8(4)	B(7)–C(2)–C(4B)	96.7(4)
C(5A)–S(2)–C(6)	108.4(3)	B(7)–B(8)–B(12)	60.0(4)	B(9)–B(12)–B(11)	108.9(4)	B(11)–C(2)–C(4B)	121.0(4)
C(2)–C(1)–B(3)	60.3(3)	B(9)–B(8)–B(12)	60.2(3)	B(10)–B(12)–B(11)	60.2(4)	C(1)–B(3)–C(2)	60.1(4)
C(2)–C(1)–B(4)	110.6(3)	B(4)–B(9)–B(5)	60.4(4)	C(2)–C(4A)–C(5A)	108.4(5)	C(1)–B(3)–B(4)	59.3(4)
B(3)–C(1)–B(4)	62.1(3)	B(4)–B(9)–B(8)	60.3(3)	C(2)–B(3)–B(4)	108.1(3)	C(1)–B(3)–B(7)	105.9(3)
C(2)–C(1)–B(5)	111.0(3)	B(5)–B(9)–B(8)	108.3(5)	C(2)–B(3)–B(7)	57.8(4)	B(4)–B(3)–B(7)	108.9(4)
B(3)–C(1)–B(5)	113.8(4)	B(4)–B(9)–B(10)	107.6(4)	C(1)–B(3)–B(8)	104.6(3)	C(2)–B(3)–B(8)	104.8(3)
B(4)–C(1)–B(5)	63.4(3)	B(5)–C(9)–B(10)	58.8(4)	B(4)–B(3)–B(8)	59.8(4)	C(2)–C(4B)–C(5B)	95.3(6)
C(2)–C(1)–B(6)	61.5(3)	B(8)–B(9)–B(10)	108.2(5)	B(7)–B(3)–B(8)	60.0(3)	C(1)–B(4)–B(3)	58.6(3)
B(3)–C(1)–B(6)	113.4(4)	B(4)–B(9)–B(12)	109.1(4)	C(1)–B(4)–B(5)	57.6(4)	S(2)–C(5A)–C(4A)	109.4(6)
B(4)–C(1)–B(6)	115.0(3)	B(5)–B(9)–B(12)	107.5(3)	B(3)–B(4)–B(5)	106.3(5)	C(1)–B(4)–B(8)	105.2(3)
B(5)–C(1)–B(6)	62.6(3)	B(8)–B(9)–B(12)	60.9(4)	B(3)–B(4)–B(8)	61.2(3)	B(5)–B(4)–B(8)	106.1(4)
C(2)–C(1)–C(11A)	124.6(4)	B(10)–B(9)–B(12)	59.8(4)	C(1)–B(4)–B(9)	103.7(3)	B(3)–B(4)–B(9)	107.4(4)
B(3)–C(1)–C(11A)	132.1(3)	B(5)–B(10)–B(6)	61.1(5)	B(5)–B(4)–B(9)	59.2(4)	S(2)–C(5B)–C(4B)	95.2(8)
B(4)–C(1)–C(11A)	121.9(3)	B(5)–B(10)–B(9)	59.5(4)	B(8)–B(4)–B(9)	58.8(4)	C(1)–C(5)–B(4)	59.1(3)
B(5)–C(1)–C(11A)	107.4(3)	B(6)–B(10)–B(9)	108.7(5)	C(1)–B(5)–B(6)	59.7(3)	B(4)–B(5)–B(6)	109.2(4)
B(6)–C(1)–C(11A)	106.5(4)	B(5)–B(10)–B(11)	109.0(4)	C(1)–B(5)–B(9)	105.8(3)	S(2)–C(6)–C(7)	117.1(8)
C(2)–C(1)–C(11B)	100.7(5)	B(6)–B(10)–B(11)	60.8(4)	B(4)–B(5)–B(9)	60.4(3)	C(6)–C(7)–O	110.8(6)
B(3)–C(1)–C(11B)	85.6(4)	B(9)–B(10)–B(11)	107.6(3)	B(6)–B(5)–B(9)	108.6(4)	C(9)–C(8)–O	110.4(3)
B(4)–C(1)–C(11B)	110.2(4)	B(5)–B(10)–B(12)	107.7(4)	C(1)–B(5)–B(10)	105.5(5)	S(1)–C(9)–C(8)	116.9(4)
B(5)–C(1)–C(11B)	147.9(4)	B(6)–B(10)–B(12)	109.2(4)	B(4)–B(5)–B(10)	109.8(4)	B(6)–B(5)–B(10)	58.8(3)
B(6)–C(1)–C(11B)	134.8(4)	B(9)–B(10)–B(12)	59.3(3)	S(1)–C(10A)–C(11A)	108.9(4)	B(9)–B(5)–B(10)	61.6(4)
B(11)–B(10)–B(12)	60.1(4)	C(1)–C(2)–B(3)	59.6(3)	C(1)–B(6)–C(2)	58.9(3)	C(1)–B(6)–B(5)	57.7(5)
C(2)–B(11)–B(6)	60.5(3)	C(1)–C(2)–B(6)	59.6(4)	C(2)–B(6)–B(5)	105.1(3)	C(1)–B(6)–B(10)	104.9(5)
C(2)–B(11)–B(7)	58.6(3)	B(3)–C(2)–B(6)	111.1(3)	C(2)–B(6)–B(10)	105.2(4)	B(5)–B(6)–B(10)	60.0(5)
B(6)–B(11)–B(7)	108.5(4)	C(1)–C(2)–B(7)	110.3(4)	C(1)–B(6)–B(11)	105.3(3)	S(1)–C(10B)–C(11B)	108.5(3)
C(2)–B(11)–B(10)	104.9(4)	B(3)–C(2)–B(7)	63.9(3)	C(2)–B(6)–B(11)	57.5(4)	B(5)–B(6)–B(11)	108.5(5)
B(6)–B(11)–B(10)	57.9(4)	B(6)–C(2)–B(7)	113.1(4)	B(10)–B(6)–B(11)	61.2(4)	C(1)–C(11A)–C(10A)	108.2(5)
B(7)–B(11)–B(10)	108.0(4)	C(1)–C(2)–B(11)	109.5(3)	C(2)–B(7)–B(3)	58.4(4)	C(2)–B(7)–B(8)	105.2(4)
C(2)–B(11)–B(12)	105.3(5)	B(3)–C(2)–B(11)	114.5(4)	B(3)–B(7)–B(8)	59.8(5)	C(2)–B(7)–B(11)	58.6(4)
B(6)–B(11)–B(12)	106.5(4)	B(6)–C(2)–B(11)	62.0(3)	B(3)–B(7)–B(11)	106.8(3)	B(8)–B(7)–B(11)	107.7(4)
B(7)–B(11)–B(12)	60.5(3)	B(7)–C(2)–B(11)	62.8(3)	C(2)–B(7)–B(12)	105.0(3)	C(1)–C(11B)–C(10B)	95.3(6)
B(10)–B(11)–B(12)	59.7(4)	C(1)–C(2)–C(4A)	111.6(4)	B(3)–B(7)–B(12)	106.8(4)	B(8)–B(7)–B(12)	59.5(3)
B(7)–B(12)–B(8)	60.5(4)	B(3)–C(2)–C(4A)	127.6(4)	B(11)–B(7)–B(12)	60.1(3)	B(3)–B(8)–B(4)	59.0(4)
B(7)–B(12)–B(9)	107.8(5)	B(6)–C(2)–C(4A)	102.5(4)	B(3)–B(8)–B(7)	60.2(4)	C(7)–O–C(8)	111.4(3)
B(8)–B(12)–B(9)	58.8(4)	B(7)–C(2)–C(4A)	134.7(4)	B(4)–B(8)–B(7)	108.5(4)		
B(7)–B(12)–B(10)	107.4(3)	B(11)–C(2)–C(4A)	116.5(4)				

flask (250 cm^3) fitted with a dinitrogen inlet/outlet, containing dry bis(2-methoxyethyl) ether (diglyme, 40 cm^3) was added 1,2-dicarba-*closo*-dodecaborane (2 g, 13.9 mmol). The mixture was cooled (ice-water) during the addition of *n*-butyllithium (9.0 cm^3, 14.4 mmol). After stirring for 1 h, ethylene sulfide (2 cm^3) was added. The mixture was allowed to stir at room temperature for 4 h. A white precipitate separated, and the solution became red. The suspension was cooled once more to 0 °C then 1 mol dm^{-3} HCl (40 cm^3) was added. Stirring was continued for 20 min, before extraction with chloroform (20 cm^3). The aqueous phase was washed with chloroform (2 × 10 cm^3), the chloroform extracts were combined, dried and evaporated under vacuum; to the residue, diethyl ether (10 cm^3) and tetrahydrofuran (4 cm^3) were added, and the solution was chromatographed on alumina, using diethyl ether–tetrahydrofuran (5:2) as eluent. After partial evaporation of the solvent, and on standing, white crystals of the dithiol compound **9** appeared. Yield 1.75 g (64%) (Found: C, 27.5; H, 7.9. $C_6H_{20}B_{10}S_2$ requires C, 27.3; H, 7.6%); FTIR (KBr), ν_{max} 2941 (C–H), 2564 (B–H), 1441, 1384 cm^{-1}[δ(C–H)]. NMR (25 °C): δ_H(400 MHz, $CDCl_3$, $SiMe_4$): 1.55 (t, J = 7.9, 2 H, SH), 2.43 (t, J = 8.4, 4 H, $BCCH_2$), 2.66 (unresolved apparent q, apparent J = 7.9, 4 H, CH_2S); δ_C(100.57 MHz, $CDCl_3$, $SiMe_4$) 23.29 (s, $BCCH_2$), 39.34 (s, CH_2SH), 77.92 (s, BC); δ_B(128.4 MHz, $CHCl_3$, BF_3·Et_2O) − 4.75 [d, ^1J(BH) 142.50, 2B], − 10.44 [d, ^1J(BH) 136.50, 4B], − 11.39 [d, ^1J(BH) 136.99 Hz, 4B]. This compound was used directly for the synthesis of **4** as described below.

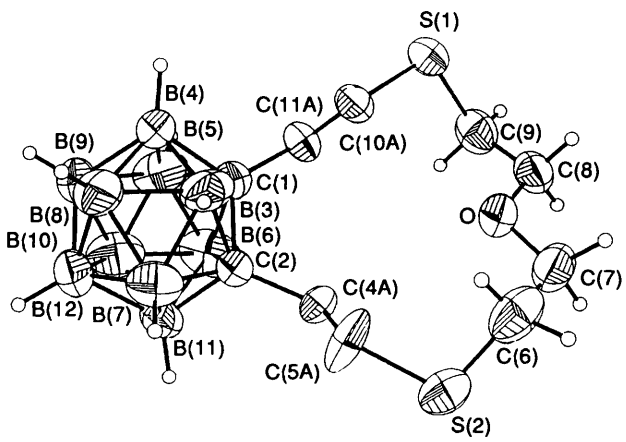

Fig. 18 View of one of the multiple possible conformers of **4** drawn using ORTEP[30] and showing the atomic numbering used. Hydrogen atoms have been omitted from the disordered section for clarity

Preparation of 1,2-(6′-*Oxa*-3′,9′-*dithiaundecane*-1′,11′-*diyl*)-1,2-*dicarba*-closo-*dodecaborane*, **4**.—Under a dinitrogen atmosphere, 1,2-bis(2-mercaptoethyl)-1,2-dicarba-*closo*-dodecaborane (0.25 g, 0.95 mmol) was dissolved in degassed absolute ethanol (50 cm^3). 3-Oxapentanediyl bis(toluene-*p*-sulfonate) (0.19 g, 0.46 mmol) was dissolved in ethanol–tetrahydrofuran (35:15). By means of a syringe pump, the dicarbaborane and

the ditosylate were added simultaneously from syringes at a rate of 4 cm^3 h^{-1} onto refluxing degassed absolute ethanol (300 cm^3), contained in a round-bottom flask equipped with three condensers. To permit slow contact of the reacting solutions, the syringe tubes discharged into lateral condensers. After 2 h the addition was finished, the solvent was evaporated, and diethyl ether (30 cm^3) and sodium hydroxide (20 cm^3 of a 5 mol dm^{-3} solution) were added. The water layer was washed with more ether. The ether extract was dried over anhydrous sodium sulfate for 24 h, then evaporated. The resultant solid was dissolved in hot hexane and filtered hot. On evaporation the hexane solution yielded a white powder, which gave colourless crystals from light petroleum, yield 0.11 g (35%) (Found: C, 36.4; H, 8.0. $C_{10}H_{26}B_{10}OS_2$ requires C, 35.9; H, 7.8%). FTIR (KBr): ν_{max} 2920, 2854, 2791 (CH), 2589 (BH), 1439, 1405, 1359 (CH), 1115, 1035 cm^{-1} (CO). NMR ($CDCl_3$): δ_H($CDCl_3$) 2.64–2.67 (m, 4 H, $BCCH_2$), 2.71–2.76 (m, 8 H, CH_2SCH_2), 3.68 (apparent t, N = 9.6 Hz, 4 H, CH_2O); δ_C(100.57 MHz, 25 °C) 31.80 (s, CH_2SCH_2), 35.77 (s, $BCCH_2$), 74.49 (s, CH_2O), 78.09 (s, BC).

Crystallography.—Crystal data for **4**. $C_{10}H_{26}B_{10}OS_2$, M = 334.6, monoclinic, space group $P2_1/n$, (no. 14), a = 8.322(8), b = 14.609(4), c = 15.224(9) Å, β = 93.11(37)°, U = 1848(2) $Å^3$, Z = 4, D_c = 1.20 g cm^{-3}, $F(000)$ = 704, temperature of measurement 293 K. Crystal shape and size: prismatic, 0.4 × 0.2 × 0.15 mm. Radiation Mo-Kα, λ = 0.710 69, μ = 2.68 cm^{-1}.

Data collection and processing. Enraf–Nonius CAD4 diffractometer, number and θ range of reflections used for lattice determination = 25, 17–25°; no absorption correction applied, $[(\sin\theta/\lambda)]_{max}$ = 0.595 $Å^{-1}$; θ_{max} = 25°; $-9 < h < 9$, $0 < k < 17$, $0 < l < 18$. Number of standard reflections and their intensity variation: 3, < 1%. 3717 Reflections measured, 3235 unique, of which 892 were unobserved [$I < 2.5\sigma(I)$]. Scan method ω–2θ; scan width = 0.80 + 0.34 tanθ.

Structure analysis and refinement. The structure was solved by direct methods using MULTAN.[27] The least-squares refinement (based on F) was done with SHELX 76:[28] no. of parameters = 231, $s = \{[\Sigma w(|F_o| - |F_c|)^2/(m - n)]^{\frac{1}{2}}$; m observations, n variables$\}$ = 0.79, $w = 1/[\sigma^2(F) + 0.043F^2]$, $(s/\sigma)_{max}$ = 0.53. Final R = 0.068, R' = 0.079. The H atoms were either found in a ΔF synthesis, or placed at their calculated positions, but the coordinates were not refined. Maximum and minimum final difference Fourier peaks = 0.5 and −0.4 e $Å^{-3}$. Scattering data from ref. 29. Refined atomic coordinates are given in Table 6, and geometrical results are given in Tables 7 and 8. During the refinement, the S–C bond distances were restrained at the expected value of 1.820(8) Å, similarly, the distances C(4A)–C(5A) and C(4B)–C(5B), C(10A)–C(11A) and C(10B)–C(11B) were restrained at the value of 1.520(5) Å. The lowest R value was achieved with the following occupation factors: 0.5 for the atomic pairs C(4A)–C(5A) and C(4B)–C(5B), 0.7 for the pair C(10A)–C(11A) and 0.3 for C(10A)–C(11B). Fig. 18 shows one of the multiple possible conformations of the macrocycle.

Additional material available from the Cambridge Crystallographic Data Centre comprises H-atom coordinates and thermal parameters.

Acknowledgements

The authors are grateful for support from the SERC and by Grant No. PB87-0364 (Comisión Interministerial de Ciencia y Technologia, Spain).

References

1 N. L. Allinger, *J. Am. Chem. Soc.*, 1977, **99**, 8127.
2 U. Burkert and N. L. Allinger, *Molecular Mechanics*, American Chemical Society, Washington DC, 1982.
3 N. L. Allinger, K. Chen, M. Rahman and A. Pathiaseril, *J. Am. Chem. Soc.*, 1991, **113**, 4505 and refs. therein.
4 D. A. Pearlman and P. A. Kollman, *J. Am. Chem. Soc.*, 1991, **113**, 7167.
5 L. A. Castonguay, A. K. Rappe and C. J. Casewit, *J. Am. Chem. Soc.*, 1991, **113**, 7177.
6 K. I. Kinnear, J. C. Lockhart and D. J. Rushton, *J. Chem. Soc., Dalton Trans.*, 1990, 1365.
7 J. D. Holbrey, Ph.D. Thesis, University of Newcastle upon Tyne, 1991.
8 F. Teixidor, A. Romerosa, J. Rius, C. Miravitlles, J. Casabó, C. Viñas and E. Sanchez, *J. Chem. Soc., Dalton Trans.*, 1990, 525.
9 F. Teixidor, C. Viñas, J. Rius, C. Miravitlles and J. Casabó, *Inorg. Chem.*, 1990, **29**, 149.
10 F. Teixidor, J. Casabó, C. Viñas, L. Escriche, E. Sanchez and R. Kivekäs, *Inorg. Chem.*, 1991, **30**, 3053.
11 F. Teixidor, A. Romerosa, C. Viñas, J. Rius, C. Miravitlles, J. Casabó, *J. Chem. Soc., Chem. Commun.*, 1991, 192; F. Teixidor, J. A. Ayllon, C. Viñas, R. Kivekäs, R. Sillanpää and J. Casabó, *J. Chem. Soc., Chem. Commun.*, 1992, 1281.
12 See *Electron Deficient Boron and Carbon Clusters*, eds. G. A. Olah, K. Wade and R. E. Williams, Wiley, New York, 1991.
13 N. N. Greenwood, *Chem. Soc. Rev.*, 1992, **21**, 49.
14 R. E. Williams, *Chem. Rev.*, 1992, **92**, 177; V. I. Bregadze, *Chem. Rev.*, 1992, **92**, 209; B. Stibr, *Chem. Rev.*, 1992, **92**, 225.
15 F. H. Allen, O. Kennard and R. Taylor, *Acc. Chem. Res.*, 1983, **16**, 146.
16 CHARMm, B. R. Brooks, R. E. Bruccoleri, B. D. Olafson, D. J. States, S. Swaminathan and M. Karplus, *J. Comput. Chem.*, 1983, **4**, 187.
17 G. M. Clore, A. M. Gronenborn, G. Carlson and E. F. Meyer, *J. Mol. Biol.*, 1986, **190**, 259.
18 M. Saunders and R. M. Jarret, *J. Comput. Chem.*, 1986, **7**, 578.
19 D. J. Fuller and D. L. Kepert, *Inorg. Chem.*, 1984, **23**, 3273 and refs. therein.
20 I. Bytheway and D. L. Kepert, *J. Math. Chem.*, 1992, **9**, 161.
21 J. J. Ott and B. Gimarc, *J. Comput. Chem.*, 1986, **7**, 673.
22 H. Potenza and W. N. Lipscomb, *Inorg. Chem.*, 1966, **5**, 1471.
23 H. Potenza and W. N. Lipscomb, *Inorg. Chem.*, 1966, **5**, 1478.
24 H. Potenza and W. N. Lipscomb, *Inorg. Chem.*, 1966, **5**, 1483.
25 J. C. Lockhart and N. P. Tomkinson, *J. Chem. Soc., Perkin Trans. 2*, 1992, 533.
26 J. C. Lockhart, D. P. Mousley, M. N. S. Hill, N. P. Tomkinson, F. Teixidor, M. P. Almajano, L. Escriche, J. Casabo, R. Sillanpää and R. Kivekäs, *J. Chem. Soc., Dalton Trans.*, 1992, 2889.
27 P. Main, S. J. Fiske, S. E. Hull, L. Lessinger, G. Germain, J. P. Declercq and M. M. Woolfson, MULTAN 82, A System of Computer Programs for Automatic Solution of Crystal Structures from X-Ray Diffraction Data, Universities of York and Louvain.
28 G. M. Sheldrick, SHELX 76. Program for crystal structure determination. University of Cambridge, 1976.
29 International Tables for X-Ray Crystallography, Kynoch Press, Birmingham, 1974, vol. 4.
30 C. K. Johnson, ORTEP, Report ORNL-5138, Oak Ridge National Laboratory, Oak Ridge, TN, 1976.

Received 30*th September* 1992; *Paper* 2/05260A